The associations between El Niño–Southern Oscillation and tropical South American climate in a regional climate model

Dana McGlone[1] and Mathias Vuille[1]

Received 31 October 2011; revised 23 January 2012; accepted 3 February 2012; published 27 March 2012.

[1] High-resolution regional climate models (RCMs), run over a limited domain, are increasingly used to simulate seasonal to interannual climate variability over South America and to assess the spatiotemporal impact of future climate change under a variety of emission scenarios. These models often give a better spatiotemporal representation of climate at a regional scale; however, they are subject to errors introduced by the driving global models. Here we analyze two different simulations with the Hadley Centre Regional Climate Modeling System Providing Regional Climate for Impact Studies (PRECIS) model over tropical South America. The two simulations cover the same 30 year period (1961–1990) but were forced with different lateral boundary conditions. The first simulation was forced with the Hadley Centre Atmospheric Model version 3 (baseline), and the second was forced with European Centre for Medium-Range Weather Forecasts Re-analysis (ERA) data. Our results indicate that the ERA-forced simulation more accurately portrays seasonal temperature and precipitation, consistent with previous studies. Empirical orthogonal function and spatial regression analyses further indicate that the ERA-forced simulation more realistically simulates the El Niño–Southern Oscillation related fingerprint on interannual climate variability over South America during austral summer. The two gridded observational data sets used for model validation display large differences, which highlight significant uncertainties and errors in observational data sets over this region. In some instances the observational data quality is rivaled or even surpassed by the ERA-forced RCM results.

Citation: McGlone, D., and M. Vuille (2012), The associations between El Niño–Southern Oscillation and tropical South American climate in a regional climate model, *J. Geophys. Res.*, *117*, D06105, doi:10.1029/2011JD017066.

1. Introduction

[2] Globally averaged temperature has increased at an alarming pace over the last 150 years with a rise of ~0.75°C since the early 20th century [*Meehl et al.*, 2007]. The unprecedented rate of warming, due to increased greenhouse gas concentrations in our atmosphere, has and will continue to have a strong effect on global climate. However, the impacts will be most strongly felt at a regional to local level, which are difficult to simulate with global climate models (GCMs).

[3] Regional climate models (RCMs) have shown some success in improving our understanding of interannual and seasonal climate variability, as well as the spatiotemporal impact of future warming scenarios at the regional scale by dynamically downscaling information provided by a global climate model. A regional climate model with its higher vertical and horizontal resolution should allow for more accurate simulations of synoptic patterns affecting weather, and thus climate, than a GCM. Much of the skill of a RCM to accurately simulate climate variability over a limited domain, however, depends on the quality of the lateral boundary conditions used to drive the RCM. This dependence was demonstrated in a two-part study by *Seth and Rojas* [2003] and *Rojas and Seth* [2003] using RegCM3 nested in the Community Climate Model version 3 (CCM3) to simulate two extreme wet and dry rainfall seasons (January–May) in 1983 and 1985. Their results indicate that the regional model significantly improved the simulated monthly evolution of the extreme rainfall seasons when compared with the global model. Furthermore, the regional model RegCM3 provided much more accurate results when the lateral boundary conditions were provided by reanalysis data rather than by the CCM3 model ensemble.

[4] Here we build on these results by comparing the Providing Regional Climate for Impact Studies (PRECIS) model results over tropical South America using (1) European Centre for Medium-Range Weather Forecasts (ECMWF) reanalysis (ERA-40) data and (2) Hadley Center GCM version 3 (HadCM3) data as lateral boundary conditions. The study aims to identify the PRECIS models' biases and ability to accurately simulate present-day, December to February (DJF) precipitation and temperature from 1961 to 1990.

[1]Department of Atmospheric and Environmental Sciences, State University of New York at Albany, Albany, New York, USA.

Comparing model results from these two different simulations with observational data will help determine whether part of the model bias can be attributed to errors in the driving lateral boundary conditions, rather than poor model performance itself. Unlike *Seth and Rojas* [2003] and *Rojas and Seth* [2003], however, our focus is on the ability of the model to accurately reproduce the observed spatiotemporal associations with El Niño–Southern Oscillation (ENSO), the leading climate mode affecting tropical South America on interannual time scales. Such studies are important since the capability of the model to accurately simulate modern climatic conditions to some extent constrains its ability to accurately simulate future climate [*Urrutia and Vuille*, 2009]. This idea of course is based on the assumption that current climate teleconnections with ENSO continue to operate in the same manner under a warming scenario. Observational records over tropical South America are sparse and gridded data sets rely on data interpolation over long distances in some regions, so we rely on two independent observational data sets to assess model bias.

[5] Many observational studies have shown that ENSO is associated with preferred patterns of precipitation and temperature over tropical South America during the wet season, which coincides with DJF, over much of the domain. To our knowledge, however, this is the first study assessing the ability of a RCM to simulate the climate impacts associated with ENSO over tropical South America using two different driving data sets as lateral boundary conditions. ENSO is known to alter the position and intensity of the Hadley and Walker circulations and induce Rossby wave trains, which propagate into the subtropical and extratropical regions of South America [*Grimm*, 2003]. El Niño events are generally associated with decreased wet season precipitation over the northern part of South America and the tropical Andes, and increasing precipitation along the coastal areas of Ecuador and Peru and over the southeast. La Niña events tend to have the opposite effect [*Garreaud et al.*, 2009; *Vuille*, 1999; *Vera and Silvestri*, 2009].

[6] The first part of the study will provide a thorough quantitative evaluation of the PRECIS model performance under modern day conditions and diagnose the role played by errors introduced by the driving boundary conditions. The second part will focus on the leading climate mode affecting both temperature and precipitation during austral summer. This mode will be identified through empirical orthogonal function (EOF) analyses, and its relationship with large-scale climate variations will be diagnosed through spatial correlation and regression analyses.

2. Data and Methods

[7] The PRECIS model is an atmospheric and land surface model, which was run over the domain 13°N–30°S and 89°W–41°W. Owing to adjustments between the GCM and RCM taking place along the lateral boundaries, the domain used for analysis is reduced to 10°N–27°S and 86°W–44°W. The PRECIS model is a part of the Hadley Centre Regional Climate Modeling System, which has been run over several domains across the world including Africa, Asia, Caribbean and Central America, South America, the Middle East and Europe [e.g., *Tadross et al.*, 2005; *Bloom et al.*, 2008; *Islam et al.*, 2008; *Karmalkar et al.*, 2008, 2011; *Garreaud and Falvey*, 2009; *Islam and Rehman*, 2009; *Urrutia and Vuille*, 2009; *Marengo et al.*, 2010].

[8] The regional model is driven by the Hadley Centre Climate Model version 3 (HadCM3). In this study PRECIS was run at a ~50 km × 50 km horizontal resolution (0.44° lat × 0.44° lon). The atmosphere is resolved in 19 vertical levels from 50 m to 30 km. The model uses terrain-following sigma coordinates (σ = pressure/surface pressure) at the bottom four levels and purely pressure coordinates at the top three levels with a combination in between. In order to remain in equilibrium, the model has a time step of five minutes. Physics schemes such as dynamical flow, atmospheric sulphur cycle, clouds and precipitation, radiative processes, land surface and deep soil are described by *Jones et al.* [2004]. The model grid elevation is different from observational data sets used in this study, which introduces an additional bias over high terrain, especially when comparing surface variables such as temperature [e.g., *Urrutia and Vuille*, 2009].

[9] Two modern-day simulations were run with different lateral boundary conditions to investigate the model performance and its dependence on the driving data set. In the first simulation, run from 1960 to 1990, the lateral boundary conditions were provided by the global driving model Hadley Centre Atmospheric Model version 3P (HadAM3P). This simulation will be referred to as the baseline run (BL). In order to avoid spin-up errors caused in the first year of simulation, the year 1960 is removed from the analysis. Sea surface temperature (SST) and sea-ice extent are prescribed from observations (HadISST1) [*Rayner et al.*, 2003].

[10] The second simulation was driven with lateral boundary conditions from the European Centre for Medium-Range Weather Forecasts (ECMWF) 40-year Re-analysis (ERA-40) data from 1957 to 2001 [*Uppala et al.*, 2005] and will be referred to as the ERA run. The lateral boundary conditions are updated every 6 hours, while the surface boundary conditions are updated every day. As in the BL run, SST and sea-ice extent are prescribed from HadISST1 [*Rayner et al.*, 2003]. Here we only analyze the common period of overlap between ERA and BL, starting in 1961 and ending in 1990.

[11] We rely on two different observational data sets produced by the Climatic Research Unit (CRU TS 2.1) and the University of Delaware (UDEL), both provided on a 0.5 degree × 0.5 degree grid [*New et al.*, 2002; *Legates and Willmott*, 1990a, 1990b] to assess model bias and its ability to simulate ENSO-related interannual temperature and precipitation variability. The data from PRECIS is linearly interpolated at 0.5 degree resolution to match the observational data set's grid.

[12] Here we focus on temperature and precipitation variability from 1961 to 1990 during DJF, which coincides with the mature phase of the South American Summer monsoon [*Zhou and Lau*, 1998; *Vera et al.*, 2006; *Marengo et al.*, 2011]. Results for JJA are presented by *McGlone* [2011]. DJF represents the core of the wet season over much of the model domain and in some regions, such as the Central Andes, accounts for 50–80% of the annual total precipitation [*Vuille et al.*, 2000]. The 1961 value calculated for DJF precipitation represents the 1961–1962 season for both temperature and precipitation; hence 29 full seasons were available for analysis. For a few analyses where annual mean

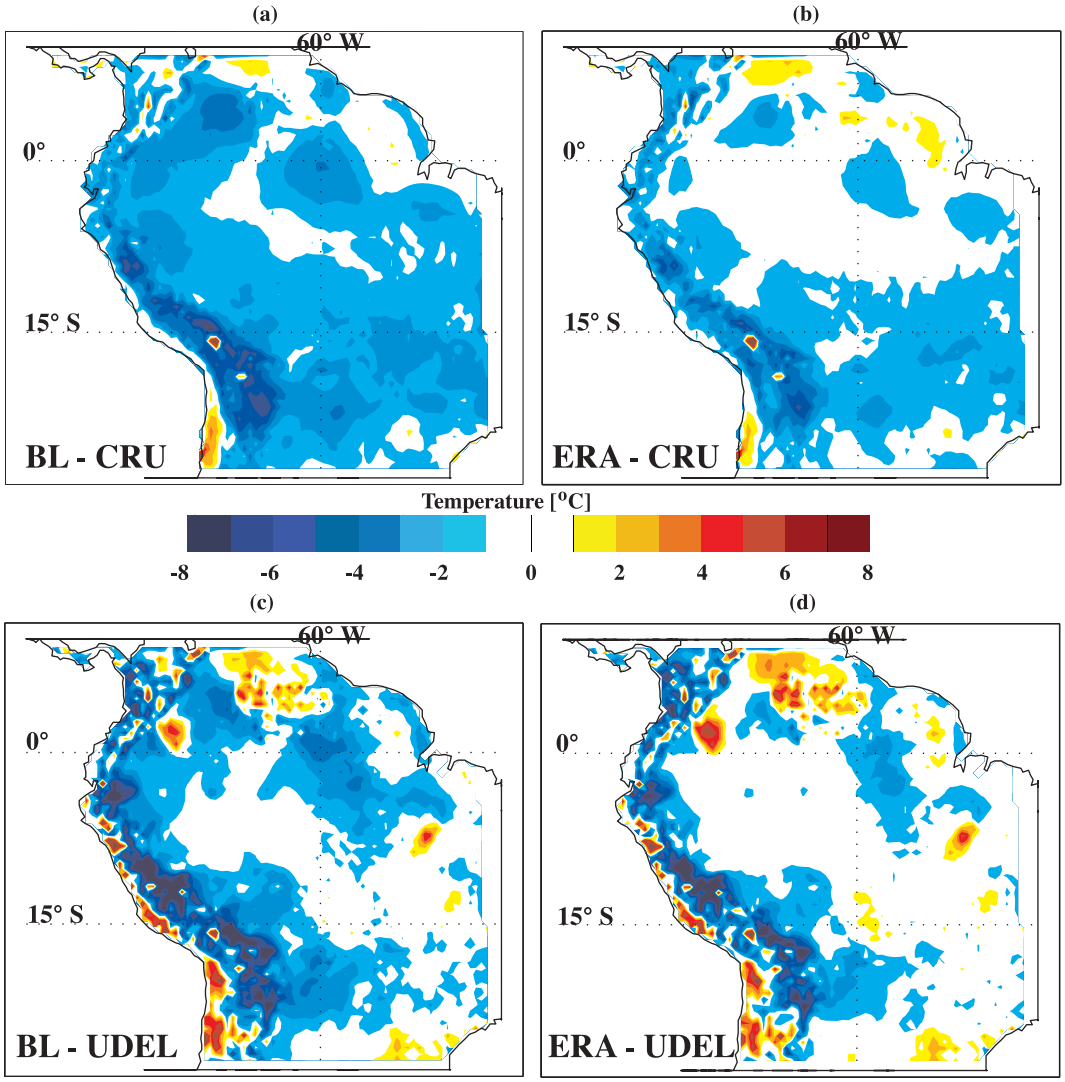

Figure 1. (a) Difference between average BL and CRU DJF temperature (1961–1990), (b) same as Figure 1a but ERA–CRU, (c) same as Figure 1a but BL–UDEL, and (d) same as Figure 1a but ERA–UDEL.

temperature and annual precipitation totals were considered, the full data over the 30 year period were used.

[13] EOFs are calculated from both observational and simulated data sets using correlation matrices of the averaged DJF precipitation and temperature anomalies in order to extract the primary modes of climate variability. Here we focus exclusively on the leading EOF, which as discussed below, is associated with ENSO variability. The lower order EOFs were not found to be associated with real, physical modes of climate variability. In an effort to make the lower order EOFs more stable and less affected by domain dependence, a varimax rotation was performed. However, the rotation of the EOFs did not improve the representation of real, physical modes of climate variability for the lower order EOFs. A more detailed discussion of the rotation and resulting modes of climate variability beyond EOF1 is given by *McGlone* [2011].

[14] In order to test the physical authenticity of the leading modes and to see whether they indeed capture ENSO-related climate variability, linear, least square fit spatial regression and Pearson correlation analyses were performed. All the correlation coefficients reported are significant at the 95% level unless noted otherwise. For the spatial regression analyses, different atmospheric and oceanic variables known to be key diagnostics to identify ENSO-related perturbations were spatially regressed with the first unrotated principal component (PC1). The influence of climate modes other than ENSO, such as the Pacific Decadal Oscillation (PDO), Tropical Atlantic Variability (TAV) and the Atlantic Multidecadal Oscillation (AMO) are described elsewhere [*McGlone*, 2011]. For this analysis we relied on gridded Extended Reconstructed Sea Surface Temperature (ERSST.v3b) at 2 degree resolution and ERA-40 850 hPa wind field and geopotential height data. Since the PRECIS lateral boundary conditions were provided by ERA-40 reanalysis data for the ERA run, we purposefully chose to use ERA-40 reanalysis data for our regression and correlation analyses rather than using a different reanalysis data set, such as National Centers for Environmental Prediction–National Center for Atmospheric Research (NCEP-NCAR) reanalysis data. Using a

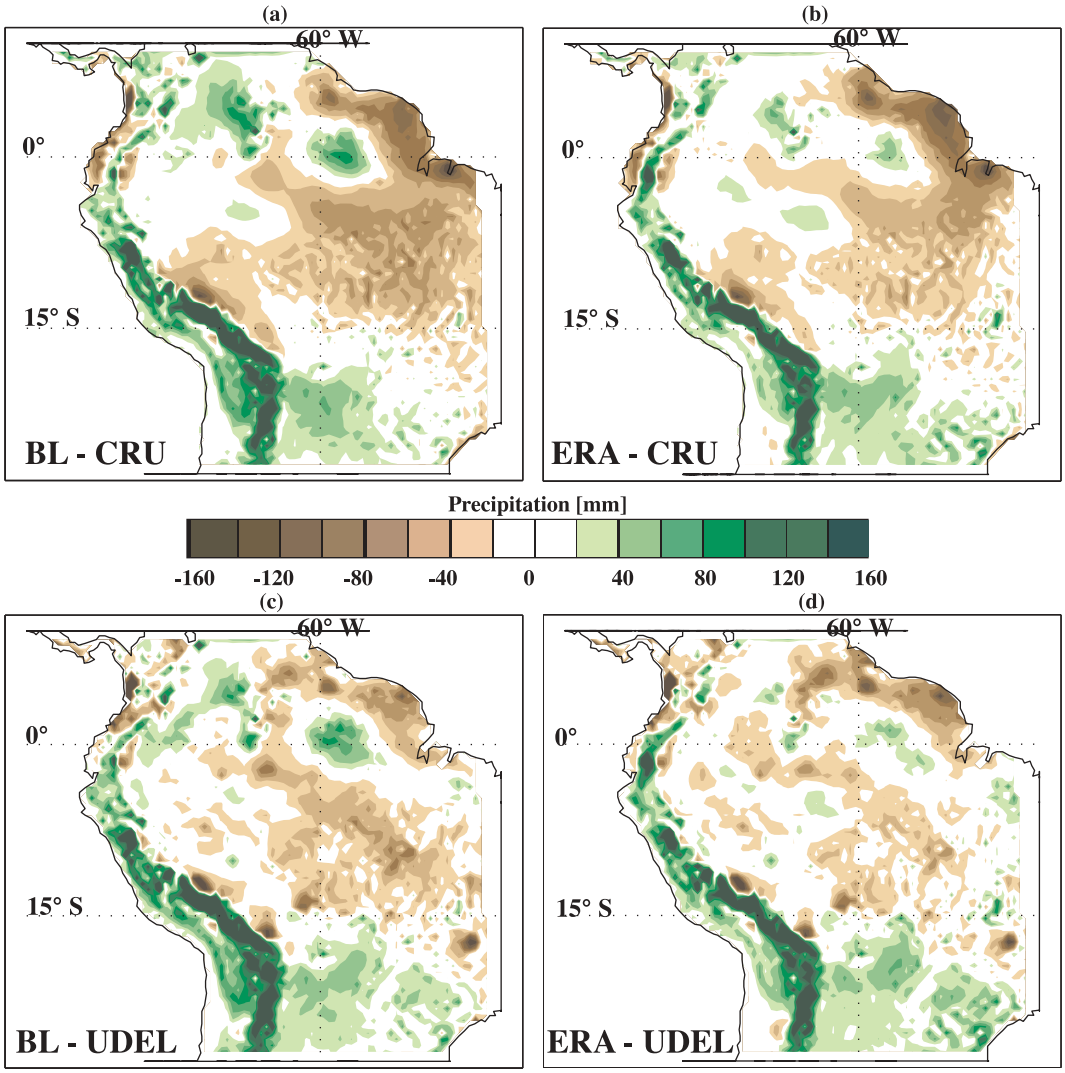

Figure 2. (a) Difference between average BL and CRU DJF precipitation (1961–1990), (b) same as Figure 2a but ERA–CRU, (c) same as Figure 2a but BL–UDEL, and (d) same as Figure 2a but ERA–UDEL.

different observational data set would have made comparison with observations more difficult to interpret [*Seth and Rojas*, 2003].

[15] Last, to independently confirm our results, a backward-spatial regression is performed in which each run's DJF temperature and precipitation data are spatially regressed against the Niño 3.4 index, describing sea surface temperature anomalies (SSTA) over the domain 120°W–170°W and 5°S–5°N [*Trenberth*, 1997].

3. Results

3.1. Seasonal Bias

[16] Figure 1 shows the DJF temperature differences between BL and CRU (Figure 1a), ERA and CRU (Figure 1b), BL and UDEL (Figure 1c), and ERA and UDEL (Figure 1d) over the 29-season period, respectively. Clearly the model shows a cold bias over much of the domain, irrespective of which observational data sets is used for comparison. This bias is consistent with the results of *Urrutia and Vuille* [2009]. However, the cold bias over the Amazon and the Andes is reduced when the model is forced with reanalysis data (Figures 1b and 1d) rather than a GCM (Figures 1a and 1c). In addition the UDEL temperature observations are more in line with the simulated DJF temperature over the lowlands than CRU, but suggest a larger model bias over the Andes. The comparison of simulated and observed temperature over the Andes, however, is complicated by the fact that the underlying grid topography is not identical. As shown by *Urrutia and Vuille* [2009], this difference accounts for a significant fraction of the apparent temperature bias over the Andes. The two small regions with a large positive temperature bias over the central Andes are related to the large lakes of Titicaca and Poopó, which are much warmer in the model simulations.

[17] Figure 2 shows the average DJF precipitation differences between models and observational data sets, respectively. The model produces excess precipitation along the eastern slopes of the Andes, while underestimating precipitation over the northeast coast and Amazon Basin.

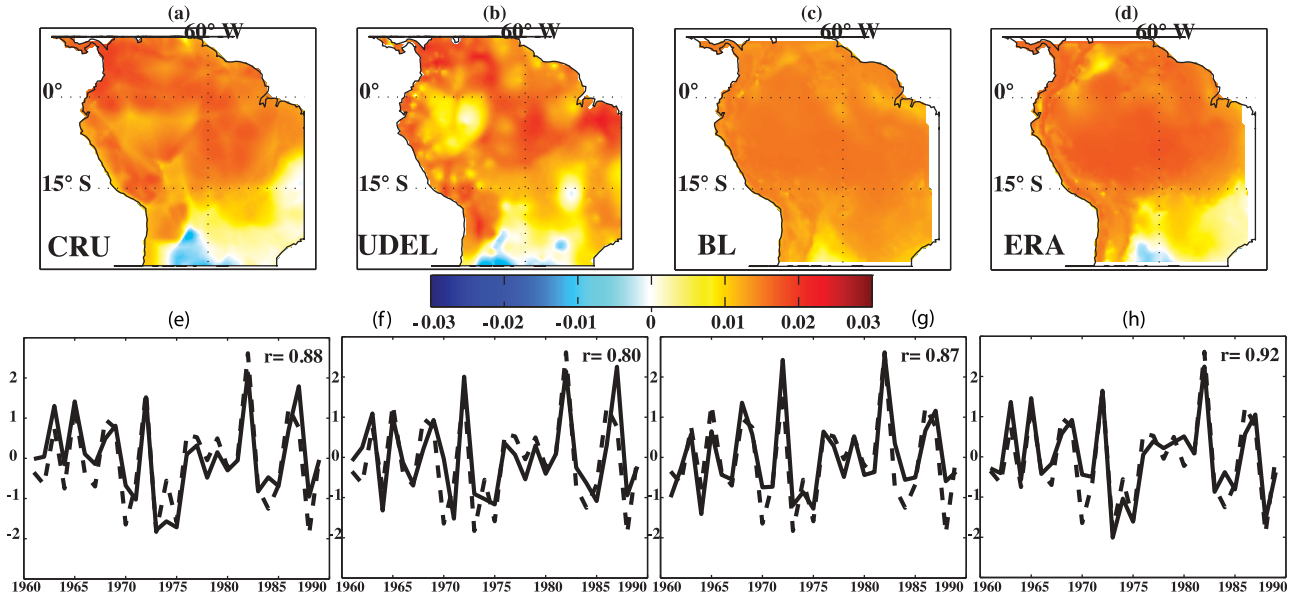

Figure 3. (a) EOF1 for CRU DJF temperature (1961–1990), (b) same as Figure 3a but for UDEL, (c) same as Figure 3a but for BL, and (d) same as Figure 3a but for ERA. (e–h) Corresponding DJF temperature principal component 1 (PC1, solid line), DJF Niño 3.4 index (dashed line), and correlation coefficients (all significant at the 95% significance level).

Overestimation of rainfall, similar to that shown along the eastern slopes of the Andes, is a common problem with RCMs in regions of steep topography [*Liang et al.*, 2004; *Frei et al.*, 2003]. However, the actual amount of precipitation over this complex terrain is not known. It is likely that the CRU and UDEL observational data sets have problems due to the lack of station data, and thus, these results should be interpreted with caution. Both BL and ERA exhibit fairly similar errors in precipitation. The PRECIS model overestimates precipitation along the Andes during the wet season by up to 800 mm or more. The close correspondence between regions of enhanced cold (Figure 1) and wet bias (Figure 2) along the eastern Andean slopes suggests they may be dynamically linked through cloud cover or soil moisture feedbacks, which will be discussed later on. The wet bias over the northern interior and along the Andes in DJF is slightly reduced with ERA. Reanalysis data also appears to slightly improve the dry bias over the majority of the interior.

[18] Consistent with the results from *Seth and Rojas* [2003] and *Rojas and Seth* [2003], the mean conditions during DJF appear to be somewhat improved when the RCM is forced with lateral boundary conditions from reanalysis data rather than from a GCM ensemble. In general our study suggests that the RCM, when driven by ERA-40 reanalysis data, shows a reduced seasonal cold bias and also a slightly reduced overestimation of wet season precipitation along the eastern Andes when compared to the GCM-forced BL simulation.

3.2. EOF Results

3.2.1. Temperature

[19] The leading EOFs (EOF1) of DJF temperature look similar, with positive loadings over the entire tropical domain (Figure 3). EOF1 for CRU, UDEL, BL and ERA explains 38.6%, 28.8%, 75.3% and 60.2% of the total variance, respectively. The loadings become negative in all data sets except BL (Figure 3c) over the subtropics east of the Andes. The loading pattern is consistent with the known large-scale association with El Niño showing uniform warming throughout the tropics. Nonetheless there is significant overestimation of this mode of variability, shown by the total variance in the RCM simulations BL and ERA (75.3% and 60.2%, respectively) when compared to the observational data sets (38.6% and 28.8%, respectively). This discrepancy suggests that the model is overestimating the relevance of the first mode, and its association with South American climate.

[20] The corresponding normalized PC1 for each EOF1 is plotted below the loading pattern (Figure 3). To highlight the fact that this leading mode is indeed related to ENSO the Niño 3.4 index, averaged over DJF, is superimposed as a dashed line. As indicated by the highly significant correlation between the two time series, there is a clear linear relationship between ENSO and EOF1 of DJF temperature (Figure 3). The leading modes for CRU, UDEL, BL and ERA have correlation coefficients with the Niño 3.4 index of 0.88, 0.80, 0.87 and 0.92, respectively. These highly positive correlation coefficients indicate significant large-scale warming (cooling) over tropical South America during El Niño (La Niña) events, which is accurately reproduced in simulations with both GCM and ERA-40 forcing. Overall, however, the ERA-driven simulation does a better job at reproducing the weaker ENSO association with temperature over the southeast and the negative relationship with El Niño over the subtropics.

3.2.2. Precipitation

[21] The leading EOFs of DJF precipitation are shown in Figure 4. CRU EOF1, which explains 18.4% of the variance (Figure 4a), displays a dipole pattern with positive loadings

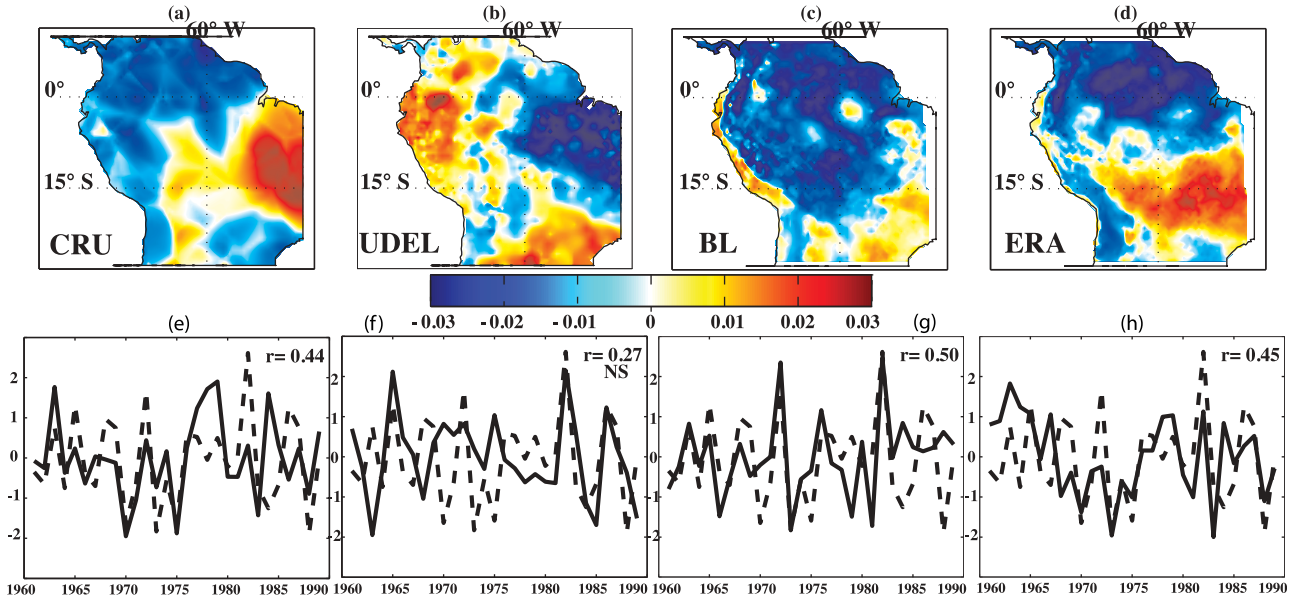

Figure 4. (a) EOF1 for CRU DJF precipitation (1961–1990), (b) same as Figure 4a but for UDEL, (c) same as Figure 4a but for BL, and (d) same as Figure 4a but for ERA. (e–h) Corresponding DJF precipitation principal component 1 (PC1, solid line), DJF Niño 3.4 index (dashed line), and correlation coefficients (all significant at the 95% significance level, except for UDEL).

in eastern Brazil and south central South America and negative loadings to the north and along the west coast. The UDEL precipitation loading (Figure 4b) appears to represent a different leading mode that explains 14.3% of the total variance. Interestingly, the first rotated EOF of the UDEL data set is much more aligned with CRU EOF1 and also shows a strong linear correlation with the Niño 3.4 index (not shown). The total variance explained by the ERA and BL EOF1 is somewhat higher than the observations (25.4% and 26.1%, respectively). The loading patterns for the BL and ERA EOF1 look more like CRU EOF1, although there are significant differences. ERA EOF1 has positive loadings extending farther to the west across subtropical South America, creating a north-south oriented dipole. BL EOF1 produces positive loadings at lower amplitude, and they are spatially restricted to the southeast of the domain. Both BL and ERA EOF1 display positive loadings along the west coast of Ecuador and Peru, a pattern that is not observed in the CRU EOF1. When compared with known precipitation anomalies associated with ENSO events, ERA EOF1 displays by far the most realistic pattern of all four leading EOFs. The CRU EOF1 associates the same mode of variability east and west of the Andes, which is not characteristic of ENSO (i.e., it does not show the "wet El Niño" pattern along the west coast). BL simulates this coastal El Niño signal, but it penetrates too far inland along the west coast up to the Andes. ERA on the other hand depicts what would be a realistic response to ENSO with a strong signal of the same sign along a narrow strip of the west coast and in southeastern South America and an opposite signal over the northeast, the Amazon basin and the tropical Andes [see *Garreaud et al.*, 2009].

[22] The comparison of the corresponding PC1s with the Niño 3.4 index confirms that the leading mode of DJF precipitation variability does have an association with ENSO (Figure 4, bottom graphs), except for the UDEL EOF1 (r = 0.27, not significant). The PC1 of CRU, BL and ERA has a correlation coefficient with Niño 3.4 of 0.44, 0.50, and 0.45, respectively. The correlation coefficients for CRU, BL and ERA precipitation indicate a weaker linear relationship with ENSO than was observed for temperature, but nonetheless they are statistically significant.

3.3. Spatial Regression

3.3.1. Temperature

[23] To further explore the relationship between ENSO and PC1, a spatial regression analysis was performed where the principal components were regressed upon various variables indicative of ENSO. The regression coefficients indicate local anomalies associated with a unit anomaly in the standardized temperature or precipitation PC. Figures 5a–5d show the spatial regression between CRU, UDEL, BL, ERA PC1, and SSTA for DJF temperature. All correlation fields show positive coefficients extending from the west coast of South America westward across the dateline with the highest values located over the central, tropical Pacific. There is another extension of the signal northeastward into the tropical North Atlantic. All spatial patterns are highly reminiscent of the canonical ENSO signature, with the typical ENSO tongue being bracketed by anomalies of the opposite sign over the mid latitudes of both hemispheres. PC1 of CRU, UDEL and ERA display the highest regression coefficients over the Niño 3.4 region, while the highest regression coefficients for BL are located slightly farther to the east over the Niño 3 index region (Figure 5c).

[24] Figure 6 shows the results of the spatial regression analysis between PC1 and the DJF 850 hPa geopotential height and wind field. All regression fields clearly reveal the

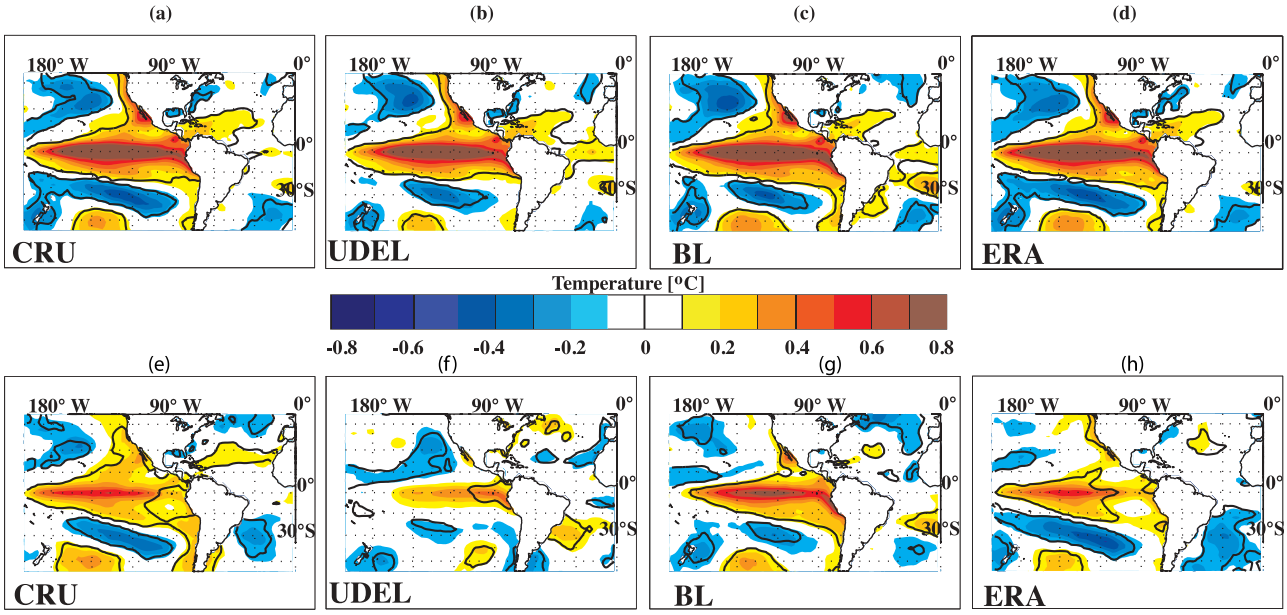

Figure 5. (a) CRU DJF temperature PC1 regressed against Extended Reconstructed Sea Surface Temperature (ERSST v3b) anomalies, (b) same as Figure 5a but for UDEL, (c) same as Figure 5a but for BL, and (d) same as Figure 5a but for ERA. (e–h) Same as Figures 5a–5d but for CRU DJF precipitation PC1. Black contour lines indicate 90% significance level of correlation coefficient.

large-scale east-west pressure dipole associated with the negative phase of the Southern Oscillation [e.g., *Trenberth and Caron*, 2000]. The trade winds over the tropical Pacific are relaxed or even reversed (westerly wind anomalies along the equator), and the subtropical jet over the North Pacific and the Caribbean is significantly strengthened, in geostrophic balance with the enhanced meridional pressure gradient. Overall, the differences between the four regression fields are minor.

3.3.2. Precipitation

[25] The spatial regression analysis for DJF precipitation PC1 with SSTA can be seen in Figures 5e–5h. The analyses

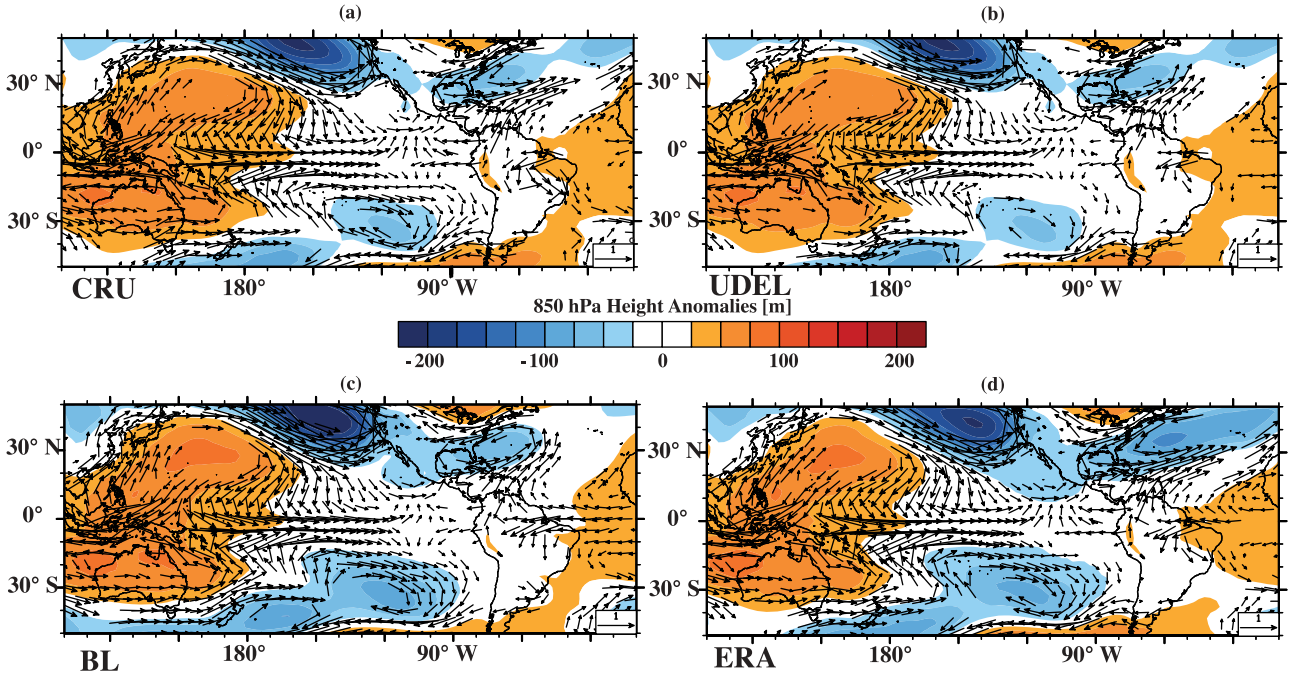

Figure 6. (a) CRU DJF temperature PC1 regressed on 850 hPa geopotential height and wind anomalies, (b) same as Figure 6a but for UDEL, (c) same as Figure 6a but for BL, and (d) same as Figure 6a but for ERA. Wind vectors are only plotted where the correlation with either the *u* or *v* component of the wind is significant at the 90% level.

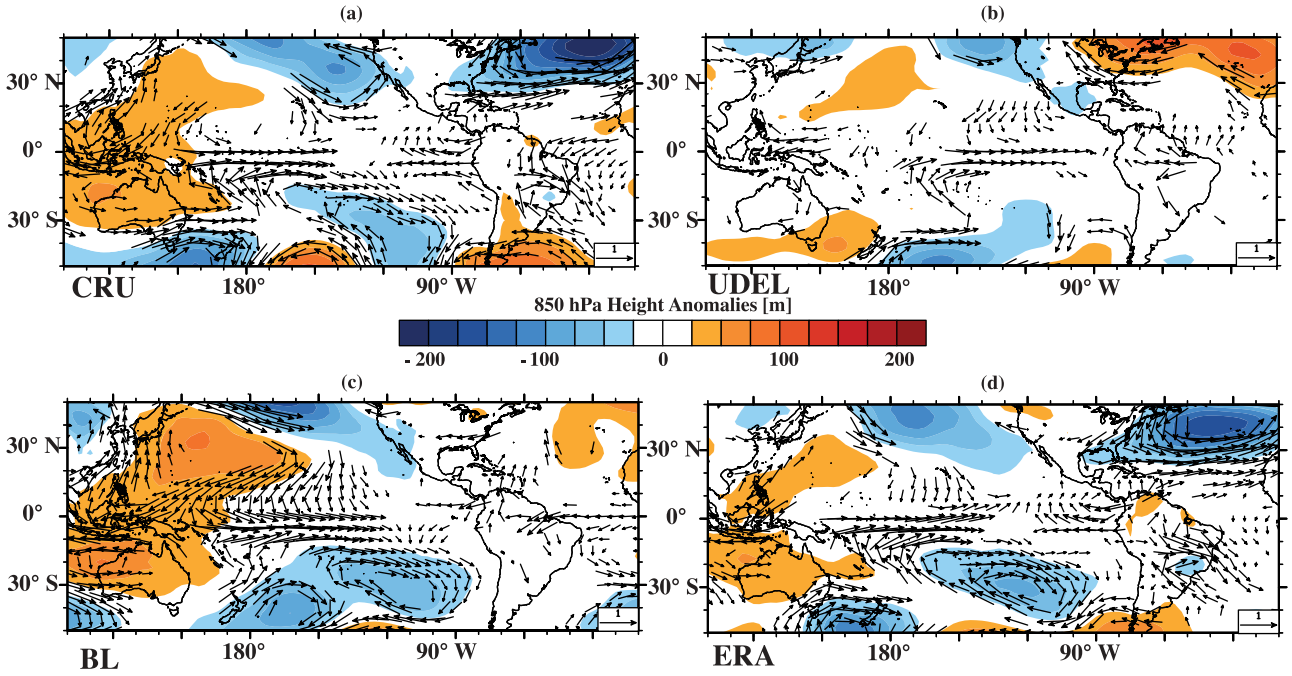

Figure 7. (a) CRU DJF precipitation PC1 regressed on 850 hPa geopotential height and wind anomalies, (b) same as Figure 7a but for UDEL, (c) same as Figure 7a but for BL, and (d) same as Figure 7a but for ERA. Wind vectors are only plotted where the correlation with either the *u* or *v* component of the wind is significant at the 90% level.

again show significant correlations and positive regression coefficients across the equatorial Pacific, except for UDEL (Figure 5f). These results suggest a clear link between ENSO and DJF precipitation variability over tropical South America as captured by the first EOF, which will be expanded on in section 3.4. Weak regression coefficients in UDEL PC1 (Figure 5f) indeed confirm that this mode does not well capture ENSO variability, as was already suggested by the low correlation coefficient with Niño 3.4 and the poor resemblance with the other EOFs (Figure 4b). However, after varimax rotation, the spatial regression between UDEL rotated PC1 and SSTA looks similar to CRU, albeit with higher-magnitude, positive loadings in the central Pacific and positive coefficients in the Atlantic (not shown). The results for BL (Figure 5g) are also somewhat different from the rest. BL projects much more strongly onto SST variability over the eastern equatorial Pacific than the other data sets, which is an overestimation of the nature of the linear relationship between Pacific SSTA and tropical South American precipitation. ERA (Figure 5h) again seems to better reproduce the relationship observed by CRU (Figure 5e) revealing strong regression coefficients over the central western equatorial Pacific. The magnitude and spatial extent of these significant regressions coefficients is slightly underestimated when compared to CRU.

[26] Figure 7 shows the regression analysis between 850 hPa geopotential height and wind field with CRU, UDEL, BL and ERA PC1 of DJF precipitation. As with temperature, the resulting large-scale regression field is reminiscent of the negative phase of the Southern Oscillation, with negative height anomalies over the southeast Pacific and positive anomalies over the western equatorial Pacific and Southeast Asia. Anomalous convergence of easterly and westerly wind anomalies over the central equatorial Pacific documents the anomalous eastward shift in the zone of deep convection during El Niño. This convection shift suggests that the leading mode of summer precipitation over tropical South America is strongly influenced by the resulting large-scale perturbations in the zonal (Walker) circulation. The result of the UDEL regression analysis again is different from the other three, showing a much weaker response in the height anomaly field and with westerly wind anomalies along the equator that are placed too far to the east (Figure 7b). As indicated before, UDEL results look similar to CRU after varimax rotation (not shown). It is also noteworthy that both UDEL and BL show positive height anomalies in their regression fields over the North Atlantic (Figures 7b and 7c), which is not present in CRU data (Figure 7a). Only ERA (Figure 7d) correctly reproduces these negative height anomalies and the anomalous cyclonic circulation over this region of the north Atlantic shown in CRU.

[27] Since the spatial regression analysis is limited to PC1 extracted from the EOF analysis, and this leading mode may not have perfectly isolated ENSO-related variability in South American precipitation and temperature data, we next explore another way to investigate the role of ENSO on DJF temperature and precipitation. We perform a backward regression, where the Niño 3.4 index (predictor) is regressed on DJF temperature and precipitation data (predictand) from the model simulations and observational data sets. Hence positive (negative) coefficients in the spatial regression fields of Figures 8–11 indicate increased (decreased) temperature or precipitation during an El Niño event and inverse conditions during a La Niña event.

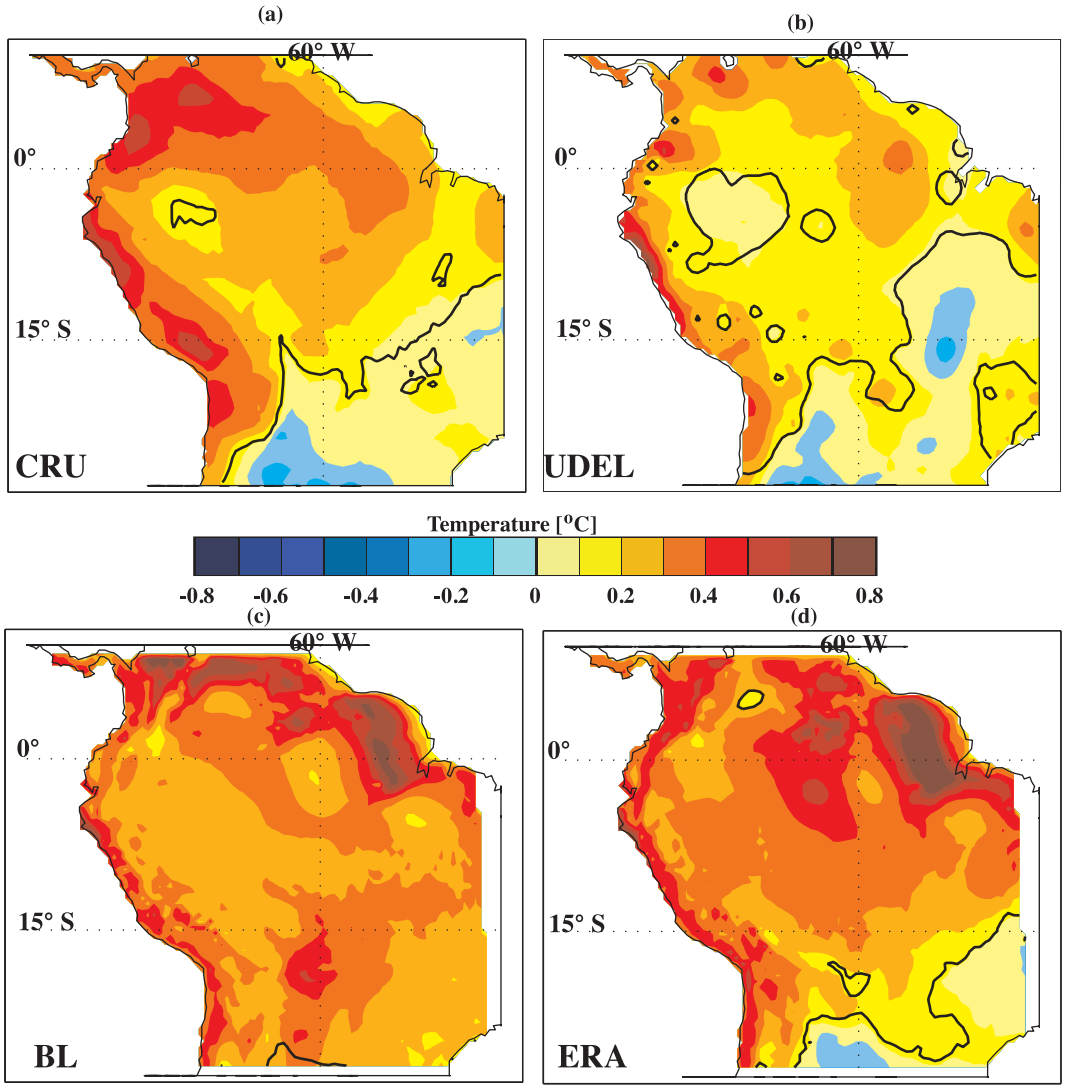

Figure 8. (a) Regression of the DJF Niño 3.4 index against CRU DJF temperature, (b) same as Figure 8a but for UDEL, (c) same as Figure 8a but for BL, and (d) same as Figure 8a but for ERA. Black contour lines indicate 90% significance level of correlation coefficient.

3.4. Backward Regression

3.4.1. Temperature

[28] Figure 8 shows the results of the UDEL, CRU, BL and ERA DJF temperature regressed against the Niño 3.4 index. Since ENSO has proven to have such a strong role shaping the leading mode of variance for seasonal temperature and precipitation, the backward regression should look similar to EOF1 and be statistically significant over the majority of the domain. The regression fields do indeed show clear similarities with the leading EOFs extracted in Figure 3, documenting that these modes are in fact depicting ENSO-related temperature variability. Positive regression coefficients dominate over almost the entire domain, indicative of the warming (cooling) of the tropical continent during El Niño (La Niña). In the central subtropics, the signal is reversed except for BL, consistent with the negative loadings in EOF 1 over this region (Figure 3c). Again ERA appears to outperform BL by correctly displaying the north-south temperature gradient shown in CRU and to a lesser extent in UDEL. The only major error in the ERA regression field occurs over NE Brazil where the temperature response to ENSO is exaggerated (Figure 8d). Warming associated with El Niño is apparent along the west coast from Colombia to Chile in all the data sets, although the signal in CRU has the largest eastward extension. Finally, while focusing on errors in the two model simulations, it is noteworthy to also point out the large differences between the two observational data sets. In fact differences between the observational data sets CRU and UDEL are as large as between CRU and ERA. For model validation it clearly matters which observational data sets is used as ground truth.

[29] Over the northeast coast, ENSO (a unit deviation in the Niño 3.4 index) accounts for ~1°C of warming in BL and ERA, which is much stronger than either observational data set suggests. Since both runs produce large, positive coefficients along the northeast coast not present in the observations, irrespective of boundary conditions used, these anomalous patterns may be related to a problem in the

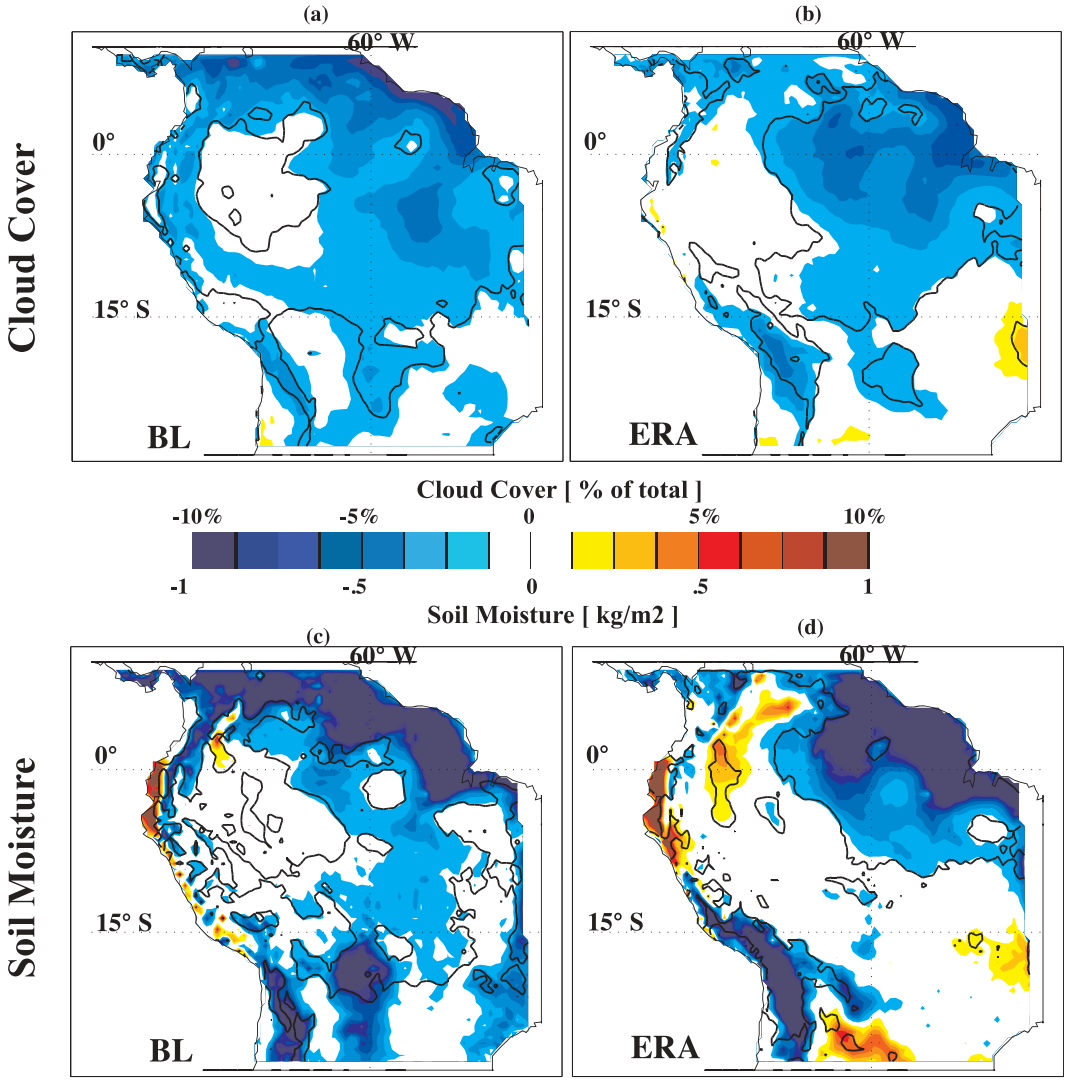

Figure 9. (a) Regression of the BL DJF cloud cover against the DJF Niño 3.4 index, (b) same as Figure 9a but for ERA, (c) regression of the BL DJF soil moisture against the Niño 3.4 index, and (d) same as Figure 9c but for ERA. Black contour lines indicate 90% significance level of correlation coefficient.

regional model itself, such as an unrealistically strong feedback mechanism, rather than caused by imperfect lateral boundary conditions.

[30] To investigate the high regression coefficients over NE Brazil in BL and ERA, the DJF Niño 3.4 index was regressed against two feedback components that are known to have the potential to amplify ENSO-related warming, DJF soil moisture and cloud cover data from the different model simulations. Indeed the regions of strongest ENSO-induced warming in NE Brazil (Figure 8) are almost identical with the areas of strongest ENSO-soil moisture coupling (Figure 9), in both BL and ERA runs. The same is, to a lesser extent, also true for the cloud-cover feedback (Figure 9). While the soil moisture coupling is indeed very relevant to set up the temperature response to ENSO [*Barreiro and Diaz*, 2011], our results suggest that soil moisture and cloud cover may provide an unrealistically high positive feedback in the model during El Niño, with strongly reduced soil moisture and cloud cover further amplifying temperature.

3.4.2. Precipitation

[31] Figure 10 shows the backward-spatial regression of DJF precipitation with the Niño 3.4 index. Significant drying over Colombia, and especially over the northeast is apparent during El Niño events in the observations from CRU and UDEL (Figures 10a and 10b). BL (Figure 10c) shows a more robust drying signal over the Colombian Andes than ERA (Figure 10d) but fails to capture the significant increase in precipitation over the southeast during El Niño events. All data sets indicate wet conditions along the coast of Ecuador and northern Peru during El Niño, but only the BL and ERA model simulations seem capable to accurately distinguish between a wet El Niño signal along the coast and a dry signal over the high Andes [*Francou et al.*, 2004]. ERA is the only data set, which accurately portrays the dry conditions on the Altiplano observed during El Niño [e.g., *Garreaud and Aceituno*, 2001; *Garreaud et al.*, 2003; *Vuille and Keimig*, 2004]. This implies higher skill in this regard than the observational data sets, which place the most arid conditions too far north and east. Overall ERA again

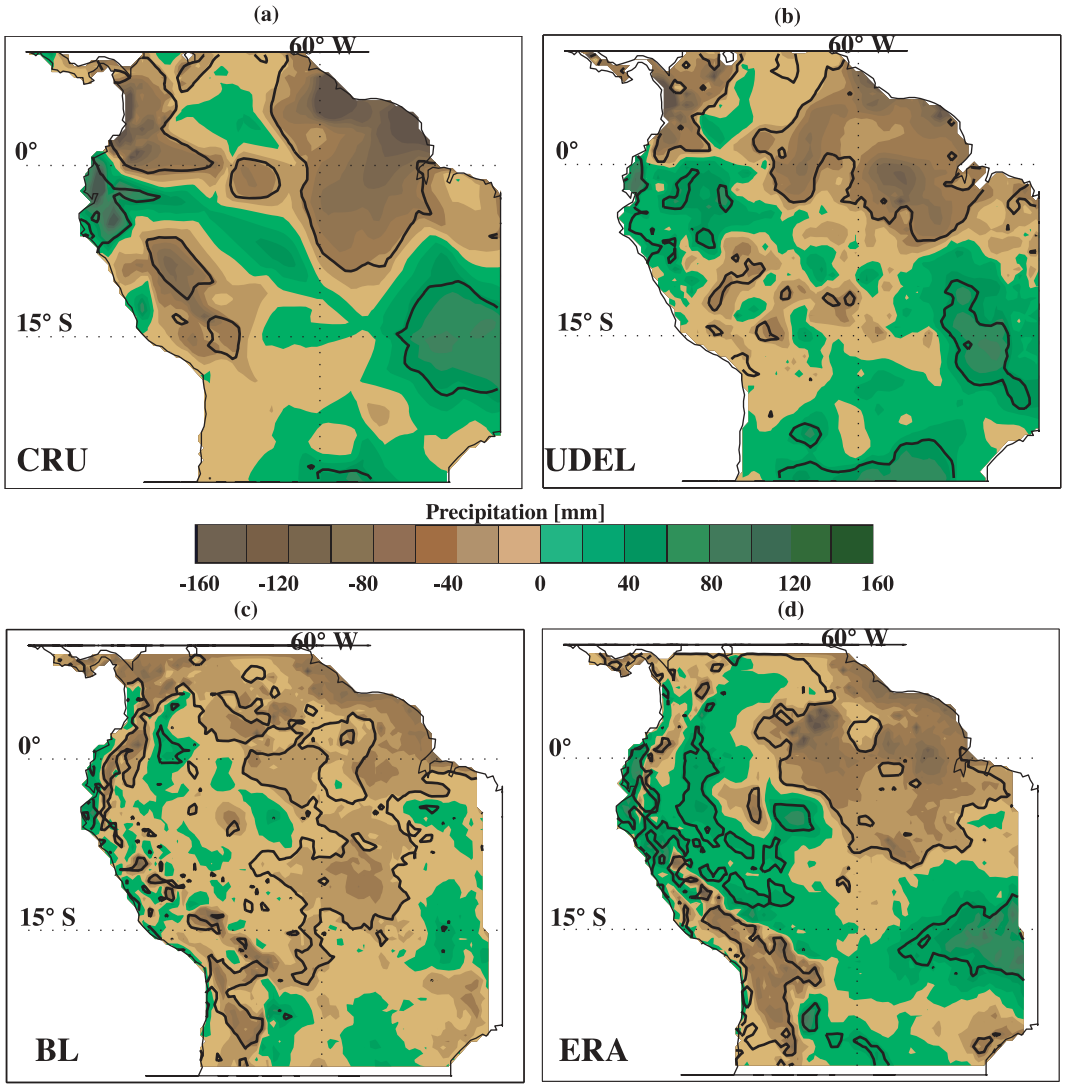

Figure 10. (a) Regression of the DJF Niño 3.4 index against CRU DJF precipitation, (b) same as Figure 10a but for UDEL, (c) same as Figure 10a but for BL, and (d) same as Figure 10a but for ERA. Black contour lines indicate 90% significance level of correlation coefficient.

performs significantly better than BL, and over regions of complex topography also appears to outperform the observational data sets.

4. Discussion

[32] Given that the two observational data sets yielded different results and both UDEL and CRU have been widely applied in observational studies over South America, it is of interest to analyze these results in some more detail. *Garreaud et al.* [2009], for example, recently performed a similar study regarding the association between ENSO and other climate modes on temperature and precipitation variability in South America using UDEL data and relying on the same spatial regression approach as in this study. However, instead of using seasonal temperature and precipitation, *Garreaud et al.* [2009] used annual averages of UDEL from 1959 to 1999 and regressed them against the Multivariate ENSO Index (MEI). The MEI is another way to measure ENSO, calculated as the first unrotated principal component over the tropical Pacific of sea level pressure, zonal and meridional components of the surface wind, SST, surface air temperature, and total cloudiness fraction [*Wolter and Timlin*, 1993]. Here we compare the results by *Garreaud et al.* [2009] to our own annual regressions between Niño 3.4 and temperature and precipitation to explore the stationarity of the ENSO fingerprint over different time periods, the changes of preferred temperature and precipitation patterns using a different measurement of ENSO and the annual versus wet season fingerprint. We will refer to the results from the *Garreaud et al.* [2009] study as UDEL2. For annual temperature, UDEL2 (Figure 11a) implies warmer (cooler) than normal conditions over tropical and subtropical latitudes during a positive (negative) MEI. As with DJF, annual temperature associations with ENSO are uniform over tropical South America. Both of the UDEL analyses (Figures 11a and 11b) look similar to each other, except the response is stronger along the northeast coast in UDEL and negative over southeastern Brazil (Figure 11b). CRU's annual temperature regression (Figure 11c) looks

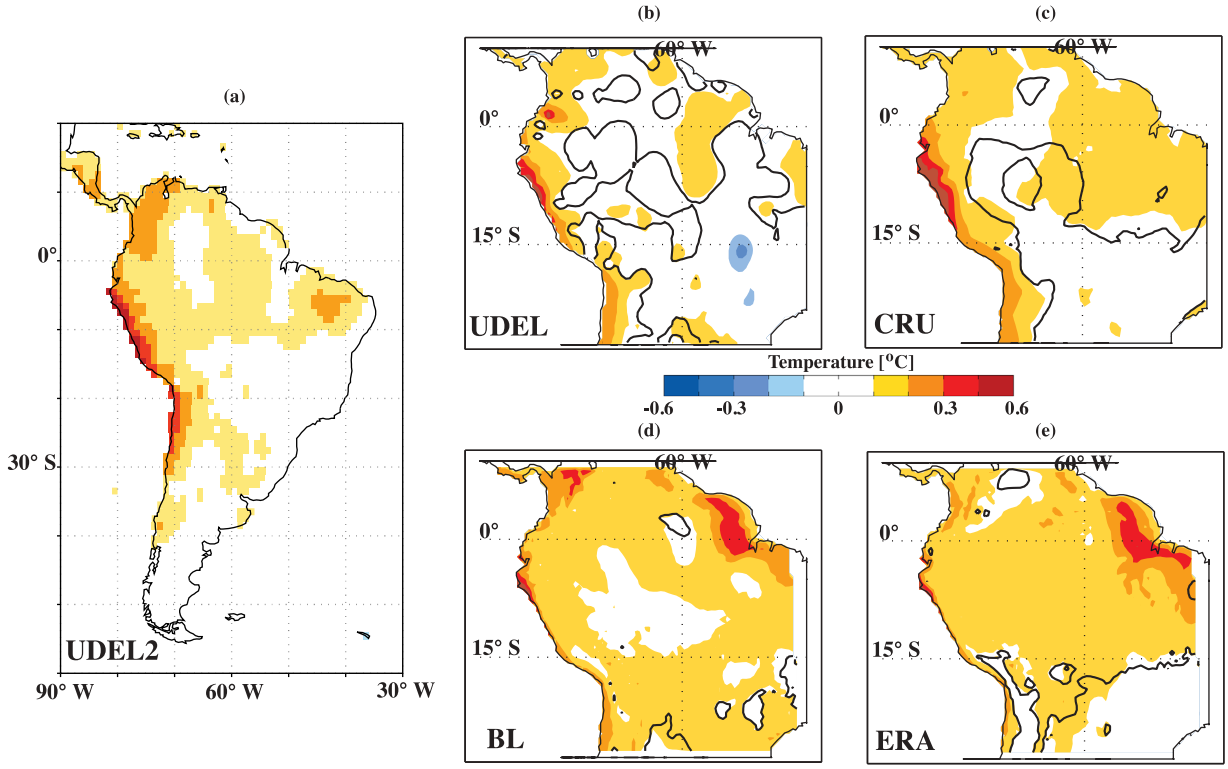

Figure 11. (a) UDEL annual mean surface air temperature regressed against MEI from 1959 to 1999 (from *Garreaud et al.* [2009], reprinted with permission from Elsevier), (b) same as Figure 11a except using Niño 3.4 index from 1961 to 1990, (c) same as Figure 11b except for CRU, (d) same as Figure 11b except for BL, and (e) same as Figure 11b except for ERA. Black contour lines indicate 90% significance level of correlation coefficient.

similar to both UDEL regressions with warming over the entire domain during a positive Niño 3.4 index. While all three observational data sets show the strongest warming occurring along the west coast, the amplitude of the warming is a bit higher in CRU. While most similar to UDEL, CRU also displays slightly stronger warming over the northeastern Amazon than both UDEL analyses.

[33] Both BL and ERA (Figures 11d and 11e) appear to overestimate the annual warming associated with El Niño over most of the domain, when compared with the observational data sets. They are notably different from observations over the northeast coast where they both show excess warming during an El Niño event. Again, this is likely related to positive feedbacks discussed earlier between Niño 3.4 and annual soil moisture and cloud cover (Figure 9). The erroneous strong warming during El Niño events over the southeast of the domain seen in the BL regression field on the other hand (Figure 11d) seems likely related to errors in the driving data set, since the simulation relying on ERA data is perfectly capable of reproducing the lack of an ENSO influence on temperature in that region (Figure 11e). When the annual ENSO fingerprint is compared to the DJF fingerprint, the main difference is the greater magnitude of warming over the Amazon Basin during DJF in CRU, BL and ERA. All the data sets indicate warming or no temperature anomaly during El Niño over the central subtropics in the annual fingerprint, whereas during DJF, all data sets except the BL-driven simulation exhibit cooling.

[34] *Garreaud et al.* [2009] likewise performed a spatial regression analysis for annual precipitation (Figure 12). Again, an updated UDEL precipitation analysis from 1961 to 1990 with the Niño 3.4 index is performed for comparison. The results in Figure 12a again suggest that tropical South America is associated with below normal precipitation during a positive MEI (El Niño) while above normal precipitation characterizes the southeastern portion of the continent, with opposite conditions prevailing during La Niña. The two UDEL analyses again look almost identical to each other indicating that the change in time period and ENSO index used is not an important factor when considering ENSO's fingerprint over tropical South America (Figures 12a and 12b). CRU captures the general drought conditions over northern South America, especially the increased drying over the northeast during El Niño and also shows positive coefficients over the southeast (Figure 12c). ENSO's effect on high-altitude precipitation is not always represented well by spatially interpolated data sets due to complex terrain, the horizontal resolution of the precipitation data and the lack of station data as input, which leads to spatial interpolation errors across regions with large precipitation gradients. An example is the coast of southern Ecuador and northern Peru, which records flood conditions at the height of an El Niño event. The positive coefficients in Ecuador are realistically restricted to the narrow coastline in UDEL and UDEL2. CRU on the other hand extends the strong positive precipitation anomalies too far inland toward the high Andes and

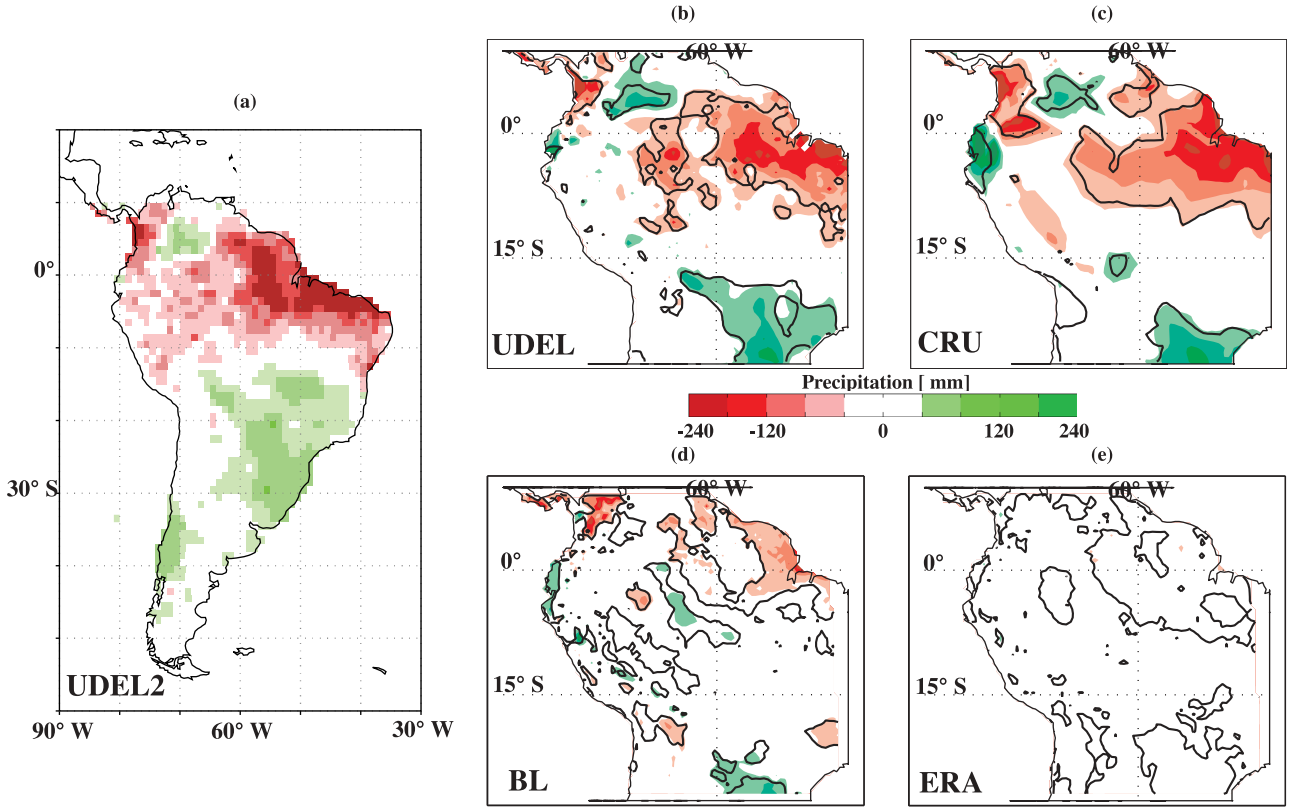

Figure 12. (a) UDEL annual mean precipitation regressed on MEI from 1959 to 1999. (from *Garreaud et al.* [2009], reprinted with permission from Elsevier), (b) same as Figure 12a except using Niño 3.4 index from 1961 to 1990, (c) same as Figure 12b except for CRU, (d) same as Figure 12b except for BL, and (e) same as Figure 12b except for ERA. Black contour lines indicate 90% significance level of correlation coefficient.

even the interior of the Amazon basin. Over the lowlands of Colombia and Venezuela, UDEL, UDEL2 and CRU all capture a significant increase in precipitation associated with El Niño events.

[35] When these observations are compared to BL and ERA, it seems that the model simulations lack a coherent, large-scale signal. ERA barely captures the overall drying trend over the north during El Niño (Figure 12e), while BL does a somewhat better job capturing the magnitude of the drying over the northeast and the Colombian Andes (Figure 12d). ERA does however display a significant change in precipitation both over the northeast and to the southeast that is spatially more like the observational data sets, but the magnitude is too weak to be displayed. BL on the other hand, correctly captures the magnitude of the ENSO-related precipitation signal to the southeast but not its full spatial extent. Using annual data eliminates the drying signal seen over the central Andes during DJF, highlighting the importance of accounting for seasonality when studying ENSO influences. Also, over the southeast, the wet signal seen in DJF is reduced and displaced farther south into the subtropics. Overall it appears as if BL is better able to reproduce the observed magnitude of the ENSO-induced precipitation anomalies, while ERA more accurately simulates the spatial significance.

[36] While both UDEL and CRU have 0.5 degree resolution, the UDEL data appears to show more fine-scale details, implying less spatial interpolation or smoothing. Clearly there appear to be some key differences in the observational data sets. Using CRU data for model validation of DJF temperature (Figure 1) shows the model having a strong cold bias over the interior Amazon basin. When using UDEL data for the same analysis, however, the cold bias produced by the models over the interior Amazon basin is small to almost negligible. Similarly UDEL data would suggest that the precipitation bias of the models is much larger with stronger drying over the interior of the continent, but no wet bias to the north when compared to CRU. Relying on UDEL data for model validation, on the other hand, improves the wet bias of the models over the Andes and implies a dry model bias along the west coast.

5. Conclusions

[37] Alongside testing the models' ability to accurately simulate the leading mode of climate variability, ENSO, under modern-day conditions, the ultimate goal of this study is to quantitatively evaluate the PRECIS model performance and diagnose the role played by errors introduced by the driving lateral boundary conditions. This analysis is crucial to better understand the model's ability and limitations in projecting future climate change for the tropical South American region [*Urrutia and Vuille*, 2009; *Marengo et al.*, 2010].

[38] This study has shown that errors in lateral boundary conditions will influence the leading modes of DJF temperature and precipitation variability as simulated by the regional model. The ERA-driven simulation produces a more realistic representation of the magnitude of these fields for DJF EOF1 when compared to the observational EOFs from CRU and UDEL. The ENSO signal in the SSTA regression field also indicates that ERA is better able to reproduce the mode captured by observations, while the BL regression analysis tends to extend the central Pacific anomalies too far east near the west coast of South America.

[39] Since the precipitation signal is more spatially complex, it comes as no surprise that both BL and ERA EOF1 have larger differences when compared to CRU and UDEL than the leading EOFs of temperature. Since UDEL captured a different leading mode, it cannot be directly compared to ERA and BL. CRU, BL and ERA all show negative coefficients over the north, but have different spatial patterns of positive loadings to the southeast. The amplitude of the positive coefficients to the southeast in BL are much less than CRU, whereas ERA has equal amplitude to CRU but extends the high-amplitude signal farther west. Even though CRU is not a model simulation but based on interpolation of actual observed data, Figure 4d shows that ERA EOF1 provides the most realistic representation of DJF precipitation's leading mode. CRU erroneously produces a mode that varies in phase east and west of the Andes and does not show the wet El Niño signal along the west coast of northern Peru and Ecuador [*Waylen and Caviedes*, 1986; *Rossel and Cadier*, 2009]. BL EOF1 on the other hand extends the wet El Niño signal along the west coast too far inland up into the Andes. A backward regression between temperature, precipitation and the Niño 3.4 index suggests that ERA again seems to do a better job at replicating the pattern and magnitude of the regression shown in the observational data sets.

[40] It is well known that the use of regional climate models, which better resolve regions of complex topography such as the Andes, improves the climatic representation on a regional scale when compared to a GCM [e.g., *Sun et al.*, 2005; *Feser et al.*, 2011]. Our study, however, even suggest that the RCM can rival the quality of gridded observational data sets in regions of poor data coverage and complex topography. However, the errors and problems within the observational data sets along the Andes make it hard to verify whether the reanalysis data and increased resolution would consistently create added value. Until there is a better observational network that addresses the inhomogeneities and data errors over the tropical Andes and South America, it is difficult to determine exactly how much added value can be gained from employing dynamically downscaled GCM output over complex terrain.

[41] The results of this study demonstrate that while dynamical downscaling of GCM output has some limitations, these shortcomings improve when using reanalysis data as boundary conditions. Many of the regional climate model inaccuracies and biases, however, relate back to the model parameterizations and model physics. Despite these limitations, there is still a role for dynamical downscaling studies using future emission scenarios. Creating ensembles using several GCM-RCM combinations or comparing results with studies that rely on statistical downscaling are additional avenues to reduce uncertainties in future regional-scale climate change projections.

[42] Using two observational data sets helps to better evaluate the model performance and presents some interesting results regarding the quality of observational gridded data products over tropical South America. Both observational data sets seem to have strengths and weaknesses. The inconsistencies in the data sets most likely arise from difficulties in data access, nondigitized records, inhomogeneities, and presence of data errors [*Garreaud et al.*, 2009]. These errors are most likely exacerbated over the Andes and Amazon Basin where sparse data, discontinuous records and complex topography with strong climatic gradients can lead to interpolation errors.

[43] A few assumptions were made in order to perform the analyses in this study. Although the leading EOF was shown to capture ENSO, some error may arise in the EOF loadings from the simulation errors associated with, for example, PRECIS' overestimate of precipitation along the eastern slopes of the Andes. Also, both the correlation and regression analyses implicitly assume a linear relationship between ENSO and the two variables temperature and precipitation. ENSO's effect on temperature and precipitation is not always best described with a linear relationship, but over this region it is a reasonable first-order assumption [*Garreaud et al.*, 2009]. There are also different spatiotemporal characteristics associated with each ENSO event, so the Niño 3.4 index and the MEI may not capture every individual ENSO event to the same extent. Nonetheless, the comparison of our results with those obtained by *Garreaud et al.* [2009] using annual temperature and precipitation data suggest that over the past 50 years, it matters little which index is used to describe the climatic impacts over tropical South America. Similarly the choice of time period (1950–99 versus 1961–90) does not appear to dramatically alter the results, suggesting that ENSO's influence on tropical South American climate was stationary over this period. Seasonality seems to be important, as there were some differences in the regression fields of temperature and precipitation with ENSO between annual and DJF time scales.

[44] This study explores the contemporaneous relationship between temperature, precipitation and ENSO without taking into account a potential lead-lag relationship with the climate indices. While the analyses between the ENSO indices and climate variables over tropical South America yielded significant results, they might have produced an even stronger relationship if a lag between ENSO forcing and climate response had been introduced. For example tropical Pacific SSTA are known to lead the temperature response over the tropical Andes by 1–2 months [*Vuille et al.*, 2000].

[45] Since this model has been used to simulate future climate change over the same domain [*Urrutia and Vuille*, 2009; *Marengo et al.*, 2010], the results produced here may also be relevant for the discussion of how potential future changes in ENSO characteristics might impact climate over South America. A big question mark in this regard is the whether the relationship between ENSO, temperature and precipitation over tropical South America as presented here, will remain stationary.

[46] **Acknowledgments.** This study forms part of the M.S. thesis of D.M. at the University at Albany. Model runs were performed at the University of Massachusetts under NSF awards EAR-0519415 and EAR-0836215 to M.V. Additional funding was provided by the U.S. State Department, Bureau of Western Hemisphere Affairs, through award S-LMAQM-11-GR-086. We would like to thank the ECMWF for the ERA-40 data and www.esrl.noaa.gov/psd/data/climateindces/list for the Niño indices. The NOAA_OI_SST_V2 data were provided by the NOAA/OAR/ESRL PSD, Boulder, Colorado, USA, from their Web site at http://www.esrl.noaa.gov/psd.

References

Barreiro, M., and N. Diaz (2011), Land-atmosphere coupling in El Nino influence over South America, *Atmos. Sci. Lett.*, *12*, 351–355, doi:10.1002/asl.348.

Bloom, A., V. Kotroni, and K. Lagouvardos (2008), Climate change impact of wind energy availability in the Eastern Mediterranean using the regional climate model PRECIS, *Nat. Hazards Earth Syst. Sci.*, *8*, 1249–1257, doi:10.5194/nhess-8-1249-2008.

Feser, F., B. Rockel, H. von Storch, J. Winterfeldt, and M. Zahn (2011), Regional climate models add value to global model data, *Bull. Am. Meteorol. Soc.*, *92*(9), 1181–1192, doi:10.1175/2011BAMS3061.1.

Francou, B., M. Vuille, V. Favier, and B. Cáceres (2004), New evidence for an ENSO impact on low-latitude glaciers: Antizana 15, Andes of Ecuador, 0°28′S, *J. Geophys. Res.*, *109*, D18106, doi:10.1029/2003JD004484.

Frei, C., J. H. Christensen, M. Déqué, D. Jacob, R. G. Jones, and P. L. Vidale (2003), Daily precipitation statistics in regional climate models: Evaluation and intercomparison for the European Alps, *J. Geophys. Res.*, *108*(D3), 4124, doi:10.1029/2002JD002287.

Garreaud, R. D., and P. Aceituno (2001), Interannual rainfall variability over the South American Altiplano, *J. Clim.*, *14*, 2779–2789, doi:10.1175/1520-0442(2001)014<2779:IRVOTS>2.0.CO;2.

Garreaud, R., and M. Falvey (2009), The coastal winds off western subtropical South America in future climate scenarios, *Int. J. Climatol.*, *29*, 543–554, doi:10.1002/joc.1716.

Garreaud, R., M. Vuille, and A. Clement (2003), The climate of the Altiplano: Observed current conditions and mechanisms of past changes, *Palaeogeogr. Palaeoclimatol. Palaeoecol.*, *194*, 5–22, doi:10.1016/S0031-0182(03)00269-4.

Garreaud, R., M. Vuille, R. Compagnucci, and J. Marengo (2009), Present-day South American climate, *Palaeogeogr. Palaeoclimatol. Palaeoecol.*, *281*, 180–195, doi:10.1016/j.palaeo.2007.10.032.

Grimm, A. M. (2003), The El Niño impact on the summer monsoon in Brazil: Regional processes versus remote influences, *J. Clim.*, *16*, 263–280, doi:10.1175/1520-0442(2003)016<0263:TENIOT>2.0.CO;2.

Islam, M. N., M. Rafiuddin, A. U. Ahmed, and R. K. Kolli (2008), Calibration of PRECIS in employing future scenarios in Bangladesh, *Int. J. Climatol.*, *28*, 617–628, doi:10.1002/joc.1559.

Islam, S., and N. Rehman (2009), Future change in the frequency of warm and cold spells durations over Pakistan simulated by the PRECIS regional climate model, *Clim. Change*, *94*, 35–45, doi:10.1007/s10584-009-9557-7.

Jones, R. G., M. Noguer, D. Hassell, D. Hudson, S. Wilson, G. Jenkins, and J. Mitchell (2004), *Generating High Resolution Climate Change Scenarios Using PRECIS*, 40 pp., Met Off. Hadley Cent., Exeter, U. K.

Karmalkar, A. V., R. S. Bradley, and H. F. Diaz (2008), Climate change scenario for Costa Rican montane forests, *Geophys. Res. Lett.*, *35*, L11702, doi:10.1029/2008GL033940.

Karmalkar, A. V., R. S. Bradley, and H. F. Diaz (2011), Climate change in Central America and Mexico: Regional climate model validation and climate change projections, *Clim. Dyn.*, *37*(3–4), 605–629, doi:10.1007/s00382-011-1099-9.

Legates, D. R., and C. Willmott (1990a), Mean seasonal and spatial variability in gauge-corrected, global precipitation, *Int. J. Climatol.*, *10*, 111–127, doi:10.1002/joc.3370100202.

Legates, D. R., and C. Willmott (1990b), Mean seasonal and spatial variability in global surface air temperature, *Theor. Appl. Climatol.*, *41*, 11–21, doi:10.1007/BF00866198.

Liang, X.-Z., L. Li, K. Kunkel, M. Ting, and J. X. L. Wang (2004), Regional climate model simulation of U.S. precipitation during 1982–2002. Part I: Annual cycle, *J. Clim.*, *17*, 3510–3529, doi:10.1175/1520-0442(2004)017<3510:RCMSOU>2.0.CO;2.

Marengo, J. A., T. Ambrizzi, R. P. da Rocha, L. M. Alves, S. V. Cuadra, M. Valverde, R. R. Torres, D. C. Santos, and S. E. T. Ferraz (2010), Future change of climate in South America in the late twenty-first century: Intercomparison of scenarios from three regional climate models, *Clim. Dyn.*, *35*(6), 1073–1097, doi:10.1007/s00382-009-0721-6.

Marengo, J. A., et al. (2011), Recent developments on the South American monsoon system, *Int. J. Climatol.*, *32*, 1–21, doi:10.1002/joc.2254.

McGlone, D. (2011), Review of the simulation of the PRECIS regional climate model over tropical South America using GCM and reanalysis lateral boundary conditions, M.S. thesis, 133 pp., State Univ. of N. Y. at Albany, Albany.

Meehl, G. A., et al. (2007), Global climate projections, in *Climate Change 2007: The Physical Science Basis. Contribution of Working Group I to the Fourth Assessment Report of the Intergovernmental Panel on Climate Change*, edited by S. Solomon et al., pp. 747–845, Cambridge Univ. Press, New York.

New, M., D. Lister, M. Hulme, and I. Makin (2002), A high-resolution data set of surface climate over global land areas, *Clim. Res.*, *21*, 1–25, doi:10.3354/cr021001.

Rayner, N. A., D. E. Parker, E. B. Horton, C. K. Folland, L. V. Alexander, D. P. Rowell, E. C. Kent, and A. Kaplan (2003), Global analyses of sea surface temperature, sea ice, and night marine air temperature since the late nineteenth century, *J. Geophys. Res.*, *108*(D14), 4407, doi:10.1029/2002JD002670.

Rojas, M., and A. Seth (2003), Simulation and sensitivity in nested modeling system for South America. Part II: GCM boundary forcing, *J. Clim.*, *16*, 2454–2471, doi:10.1175/1520-0442(2003)016<2454:SASIAN>2.0.CO;2.

Rossel, F., and E. Cadier (2009), El Niño and prediction of anomalous monthly rainfalls in Ecuador, *Hydrol. Processes*, *23*, 3253–3260, doi:10.1002/hyp.7401.

Seth, A., and M. Rojas (2003), Simulation and sensitivity in nested modeling system for South America. Part I: Reanalyses boundary forcing, *J. Clim.*, *16*, 2437–2453, doi:10.1175/1520-0442(2003)016<2437:SASIAN>2.0.CO;2.

Sun, L., D. F. Moncunill, H. Li, A. D. Moura, and F. Filho (2005), Climate downscaling over Nordeste, Brazil, using the NCEP RSM97, *J. Clim.*, *18*, 551–567, doi:10.1175/JCLI-3266.1.

Tadross, M., C. Jack, and B. Hewitson (2005), On RCM-based projections of change in southern African summer climate, *Geophys. Res. Lett.*, *32*, L23713, doi:10.1029/2005GL024460.

Trenberth, K. E. (1997), The definition of El Niño, *Bull. Am. Meteorol. Soc.*, *78*, 2771–2777, doi:10.1175/1520-0477(1997)078<2771:TDOENO>2.0.CO;2.

Trenberth, K., and J. M. Caron (2000), The Southern Oscillation revisited: Sea level pressures, surface temperatures, and precipitation, *J. Clim.*, *13*, 4358–4365, doi:10.1175/1520-0442(2000)013<4358:TSORSL>2.0.CO;2.

Uppala, S. M., et al. (2005), The ERA-40 re-analysis, *Q. J. R. Meteorol. Soc.*, *131*, 2961–3012, doi:10.1256/qj.04.176.

Urrutia, R., and M. Vuille (2009), Climate change projections for the tropical Andes using a regional climate model: Temperature and precipitation simulations for the end of the 21st century, *J. Geophys. Res.*, *114*, D02108, doi:10.1029/2008JD011021.

Vera, C., and G. Silvestri (2009), Precipitation interannual variability in South America from the WCRP-CMIP3 multi-model dataset, *Clim. Dyn.*, *32*(7–8), 1003–1014, doi:10.1007/s00382-009-0534-7.

Vera, C., et al. (2006), Toward a unified view of the American monsoon systems, *J. Clim.*, *19*, 4977–5000, doi:10.1175/JCLI3896.1.

Vuille, M. (1999), Atmospheric circulation over the Bolivian Altiplano during dry and wet periods and extreme phases of the Southern Oscillation, *Int. J. Climatol.*, *19*, 1579–1600, doi:10.1002/(SICI)1097-0088(19991130)19:14<1579::AID JOC441>3.0.CO;2-N.

Vuille, M., and F. Keimig (2004), Interannual variability of summertime convective cloudiness and precipitation in the central Andes derived from ISCCP-B3 data, *J. Clim.*, *17*, 3334–3348, doi:10.1175/1520-0442(2004)017<3334:IVOSCC>2.0.CO;2.

Vuille, M., R. S. Bradley, and F. Keimig (2000), Climate variability in the Andes of Ecuador and its relation to tropical Pacific and Atlantic sea surface temperature anomalies, *J. Clim.*, *13*, 2520–2535, doi:10.1175/1520-0442(2000)013<2520:CVITAO>2.0.CO;2.

Waylen, P. R., and C. N. Caviedes (1986), El Niño and annual floods on the north Peruvian littoral, *J. Hydrol.*, *89*, 141–156, doi:10.1016/0022-1694(86)90148-4.

Wolter, K., and M. S. Timlin (1993), Monitoring ENSO in COADS with a seasonally adjusted principal component index, paper presented at 17th Climate Diagnostics Workshop, Natl. Oceanic and Atmos. Admin., Norman, Okla.

Zhou, J., and K.-M. Lau (1998), Does a monsoon climate exist over South America?, *J. Clim.*, *11*, 1020–1040, doi:10.1175/1520-0442(1998)011<1020:DAMCEO>2.0.CO;2.

D. McGlone and M. Vuille, Department of Atmospheric and Environmental Sciences, State University of New York at Albany, 1400 Washington Ave., Albany, NY 12222, USA. (dkmcglone@gmail.com)